Current Research in Materials Chemistry

Renewable Tannin-Based Dual-Doped Carbon Material and its Application as a Supercapacitor Electrode Material

Samantha Macchi[1], Noureen Siraj[1*], Fumiya Watanabe[2], Tito Viswanathan[1]

[1]*Department of Chemistry, University of Arkansas at Little Rock, 2801 S. University Ave, Little Rock, AR 72204, USA.*

[2]*Center for Integrative Nanotechnology Sciences, University of Arkansas at Little Rock, 2801 S. University Ave, Little Rock, AR 72204, USA.*

Article Details

Article Type: Research Article
Received date: 12nd August, 2019
Accepted date: 24th September, 2019
Published date: 28th September, 2019

***Corresponding Author:** Noureen Siraj, Department of Chemistry, University of Arkansas at Little Rock, 2801 S. University Ave, Little Rock, AR 72204, USA. E-mail: nxsiraj@ualr.edu

Citation: Macchi S, Siraj N, Watanabe F, Viswanathan T (2019) Renewable Tannin-Based Dual-Doped Carbon Material and its Application as a Supercapacitor Electrode Material. Cur Res Mater Chem 1: 101. doi: https://doi.org/10.33790/crmc1100101.

Abstract

Phosphorus and Nitrogen co-Doped Carbon (PNDC) material was synthesized using a one-pot carbonization of a renewable carbon precursor, tannin (a plant-based polyphenolic oligomer) using microwave assisted-carbonization method. PNDC was characterized in detail including morphology, surface area and porosity, and elemental composition at the bulk as well as the surface. The material was found to have a high surface area (ca. 724 m^2g^{-1}) with mainly mesoporous pore distribution. Elemental functionalities on the surface and their relative abundance were analyzed in detail, since functional groups play a significant role in the formation of double layer at the surface of active material. The material showed exceptional capacitance for a biomass material at 182 Fg^{-1} in alkaline media and 156 Fg^{-1} in acidic media, thus proving to be an excellent candidate for potential use in economical supercapacitors.

Introduction

Efficient generation and storage of clean and renewable energy are becoming increasingly important as the world continues to grow in population and as the consumption of nonrenewable resources for energy needs increases. There are many methodologies to harvest renewable energy in this modern era such as solar, wind, hydrothermal and geothermal means. Oftentimes, these devices contain some form of storage device to store the energy generated. Among them, supercapacitors are a promising class of energy storage device that allows rapid and facile charge storage. Therefore, these devices are particularly useful in systems that require high amounts of energy very quickly, such as motor vehicles, power buffers, and voltage stablilizers [1,2]. These devices operate on two principles: Electric Double Layer Capacitance (EDLC) and psuedocapacitance (PC). EDLC occurs when a potential is applied over an electrode and a layer of charges of opposite polarity forms [3,4]. PC is related to specific redox reactions that take place at the electrode/electrolyte interface [5-7]. Both phenomena contribute to the overall capacitance of a material.

Capacitance of an EDL capacitor can be greatly enhanced by improving certain characteristics of the electrode coating material, such as higher surface area, conductivity, and pore size distribution [8,9]. Carbon materials are widely studied for use in EDLC, such as carbon nanotubes (CNTs) [3,10,11], aerogels [12-14], and graphene-based materials [15,16], due to their porosity. However, these often require difficult and costly synthetic routes. Among carbon-based supercapacitors, activated carbons (AC) are advantageous due to their simplistic and economical synthesis with exceptional surface areas and tunable pore sizes. AC can easily be solution processed, therefore they can be easily scaled up to industrial sized electrode production [17]. Much effort has been taken into further reduction of costs to produce ACs by using waste renewable materials as precursors. The list of renewable carbon-containing waste material is long and growing further. Some of those investigated include: used coffee [18] and tea [19], fish waste [20], and walnut shells [21]. Utilization of waste materials can reduce landfill mass and also make these electrode materials low cost. However, many of these purely carbon (and oxygen) ACs are limited in redox-capable functionalities on the surface and reduces their overall capacitance performance.

PC of carbon-based materials can be improved by tailoring the functional groups and elements present on the surface of electrode coating material [22,23]. One way to do this is to add functionalities to the surface of the materials. Many studies have been performed to increase the supercapacitance of carbon materials by doping with heteroatoms that are generally electronegative or electropositive nonmetals [24]. It has been proven that the introduction of dopant elements into the carbon matrix can alter the electrochemical properties of the material [5,25,26]. The functionalities of these additional elements can provide redox reactions capability at the surface of the material. These reversible redox reactions can enhance the overall capacitance behavior of the material by enhancing the pseudocapacitive properties. The doping elements can also enhance the capacitance by breaking the electroneutrality of the material, allowing for greater charge storage due to more overall surface charges [27]. Previous research has included the doping of porous carbon samples with heteroatoms such as boron [28], nitrogen [29,30], and silicon for capacitance enhancement [31,32].

Herein, we report the use of quebracho tannin, a plant byproduct which finds use in the petroleum extraction industry, as a renewable carbon precursor for the synthesis of Phosphorus and Nitrogen co-Doped Carbons (PNDC) material for supercapacitor application. By utilizing a one-pot microwave assisted carbonization of tannin in the presence of doping elements, high surface area doped carbon materials can be prepared. Here we report the physical and electrochemical properties of tannin-derived PNDC for supercapacitor application.

Experimental

Materials and PNDC synthesis

Quebracho tannin was obtained from Tannin Corp, Peabody, MA. Melamine, Hexamine, and Ammonium dihydrogen phosphate were purchased from Sigma. Potassium hydroxide and sulfuric acid were purchased from VWR. All chemicals were reagent grade and utilized without any further modification.

PNDC synthesis was performed in a similar manner as previously reported [33,34]. Briefly, 0.9434 g of melamine dissolved in hot DI water was mixed with 2.1630 g powdered unmodified tannin and allowed to stir, resulting in homogeneous solution (A). 4.1407 g of ammonium phosphate was then allowed to fully dissolve in the same solution. A second solution B was prepared by dissolving 0.3550 g hexamine in 5 mL DI water and was added to solution A while continuing to heat and stir until the formation of a deep brown color was apparent. The resultant brown solution was transferred to a wide evaporation dish and heated at 70 °C under a hood for 12 hours to remove water. The dried precursor material was then transferred to a boron nitride crucible with two drops of DI water, covered with a similar crucible, placed in an aluminum oxide box, and placed in a conventional microwave oven. The oven was run for 30 minutes at 2.45 GHz and 1.25 KW power and then cooled to room temperature. The carbonized product was powdered and characterized without further purification.

Characterization

Surface area/porosity analysis was performed using ASAP 2020 Micrometrics Surface Area and Porosity Analyzer with Brunauer-Emmett-Teller (BET) modeling via nitrogen adsorption/desorption isotherms at 77 K. Morphology and bulk elemental composition of the sample were analyzed using JSM-7000F Scanning Electron Microscopy (SEM) coupled with Energy Dispersive X-ray Spectroscopy (EDS). Elements and their bonding environments on the surface of the sample was studied using a Thermo K-alpha X-ray Photoelectron Spectrometer (XPS) with an Al Kα source and internal carbon standard of 284.8 eV. Raman measurements were taken using Horiba Raman Spectrometer (Jobin Yvon Lab Ram 800) with 514.5 nm laser source, 200 micrometer hole size, and ten second acquisition time.

All electrochemical measurements were performed using an EC Epsilon™ potentiostat with a typical three electrode system. Cyclic voltammetry measurements were performed in acidic (1 M H2SO4) and alkaline (6 M KOH) media with a potential window of 0.8 and 1 V, respectively. Electrolytes were purged with gaseous nitrogen for 30 minutes prior to experiments in order to ensure an inert reaction environment. Specific capacitance values were calculated using equation 1 and 2

$$C_{s,\text{cathode or anode}} = \int i(dV)/Vmv = Q/\Delta Vm = \int idt/\Delta Vm = i\Delta t/\Delta Vm \quad (1)$$

$$C_{s,\text{total}} = (C_{\text{anode}} + C_{\text{cathode}})/2 \quad (2)$$

where i is the current density, V is the potential voltage, Q is the charge, m is the mass of PNDC, and v is the scan rate.

Results/Discussion

Brunauer-Emmet-Teller (BET)

The nitrogen sorption isotherm of PNDC is classified by IUPAC as a Type IV isotherm characterized by following monolayer adsorption at low relative pressure and multilayer adsorption at higher relative pressure. This isotherm also contains a hysteresis loop, classified as a Type H4 which can be associated with narrow slit-like pore structures and its extension to lower relative pressures is indicative of micro-porosity of the material [35]. Figure 1a shows the nitrogen adsorption isotherm. Figure 1b shows the pore size distribution of PNDC, highlighting that the majority of total pore volume is comprised of pores with diameters ≤10 nm.

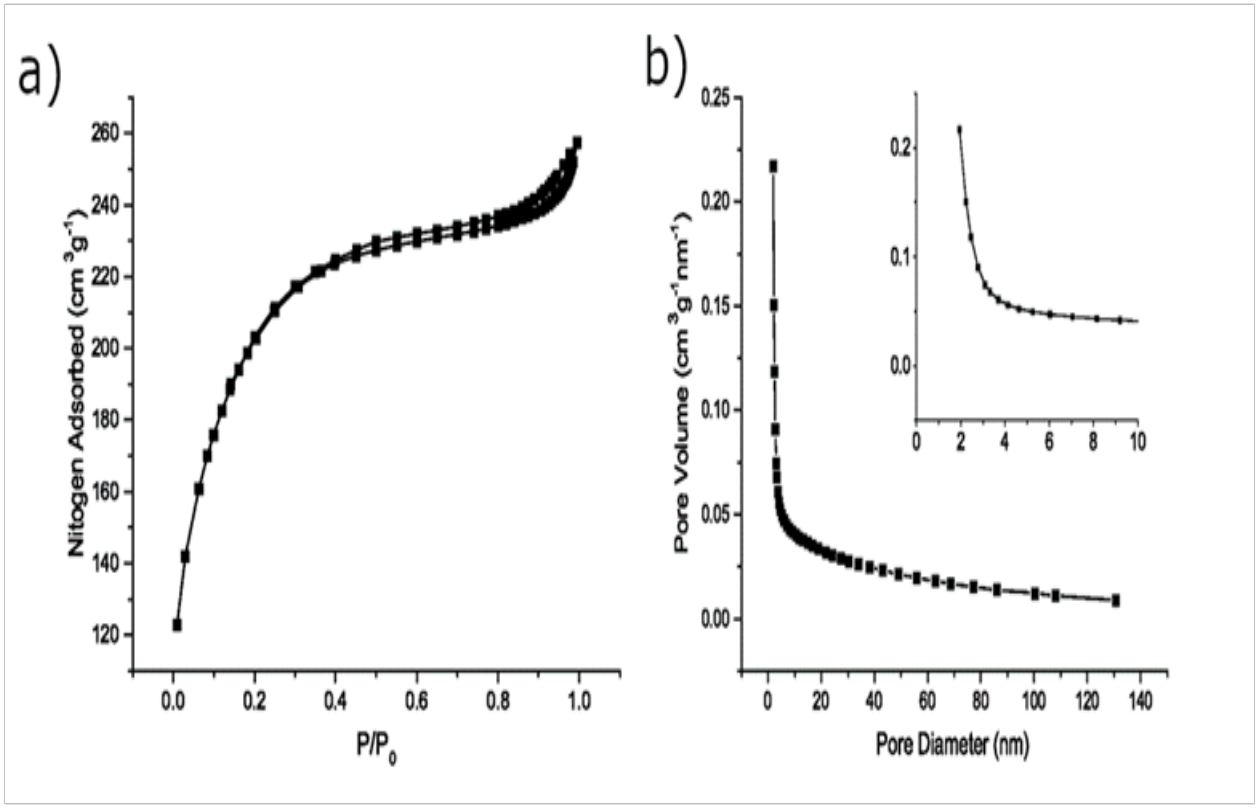

Figure.1.a) Nitrogen adsorption and desorption curves and b) pore size distribution of PNDC

PNDC shows a high BET surface area of 724.8 m^2g^{-1}. During the microwave assisted synthesis method, reducing gases are produced that create pores upon leaving the sample. This allows for a high surface area and well-developed pore structure. A sharp increase in N_2 adsorption at low relative pressure is indicative of the presence of micropores [36]. The PNDC material was also found to be comprised of 68% mesopores, which have been shown to be highly important in the charge storage process [37,38]. Detailed results of surface area and porosity analysis is tabulated in Table 1.

Sample Name	Surface Area (m^2/g)	Average Pore Width (nm)	Average BJH Pore Diameter (nm)	Pore Volume (cm^3/g)	Micropore Volume (cm^3/g)	Mesopore Volume (cm^3/g)
PNDC	724.75	2.15	3.03	0.217	0.068	0.149

Table 1.BET surface area and porosity analysis

Scanning Electron Microscopy (SEM)

SEM imaging of PNDC shows the morphology of the material, which includes spherical-shaped structures that are around 1 micron in diameter. These structures range from almost perfectly spherical to more irregular. Some of these spheres are also decorated with smaller structures (~10-80 nm) which can be seen in Figure 2a. Carbon materials with spherical morphology have shown similar surface characteristics such as high surface areas and small pore diameters (~1-5 nm) [36,39]. The repeating spherical-structured morphology correlates well with the high surface area and pore size distribution seen from BET section. Figure 2b shows the sphere-shaped morphology of PNDC at X5,000 magnification.

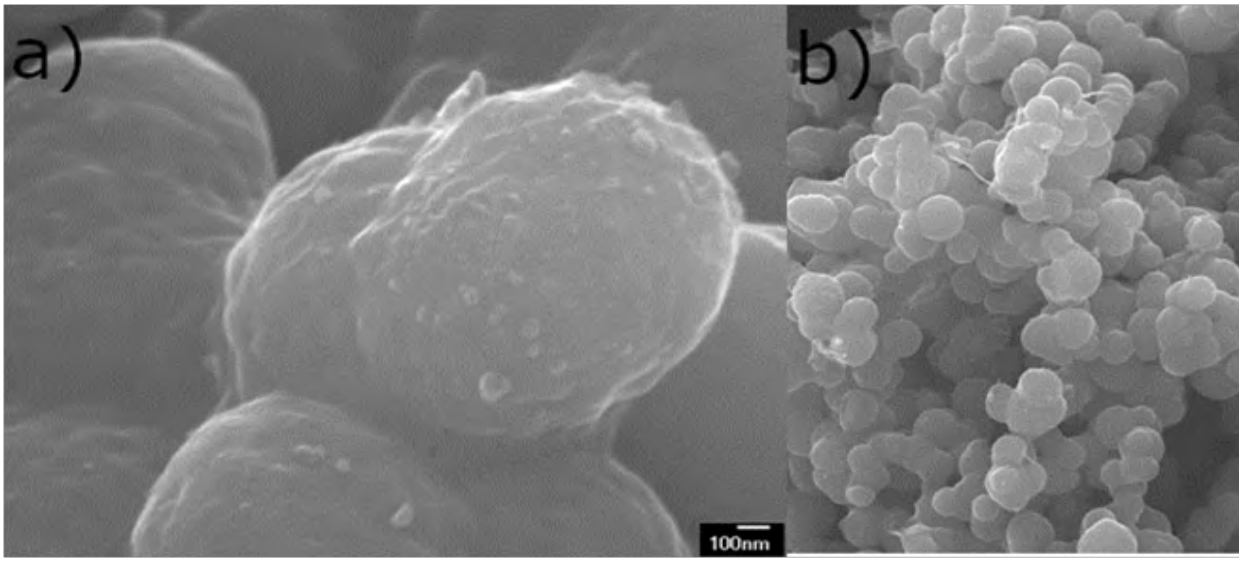

Figure.2 SEM of PNDC at a) X50,000 and b) X5,000 magnification

SEM-EDS instrumentation was utilized to analyze the bulk elemental composition of PNDC material. PNDC is mainly comprised of carbon with significant amount of oxygen and a small amount of phosphorus and nitrogen dopants. The data for elemental composition acquired from SEM-EDS is tabulated in Table 2.

Sample	C K (At%)	O K (At %)	P K (At %)	N K (At %)
PNDC	82.8	11.6	2.9	2.7

Table 2.SEM-EDSbulk elemental composition

X-Ray Photoelectron Spectroscopy (XPS)

XPS was performed to quantify the elemental composition on the surface of the PNDC material. Figure 3 shows survey scan data for PNDC material. The results showed similar results to that of EDS in that the sample contains mostly carbon and oxygen with varying amounts of phosphorus and nitrogen. However, the surface of PNDC is much richer with heteroatom doping elements. This is attributed to the microwave process localizing heavier non-carbon atoms onto the surface during synthesis.

Narrow scan analysis of the data provides not only the percent elemental composition, but it also suggests the functionalities of different heteroatoms in PNDC. This data is essential for a better

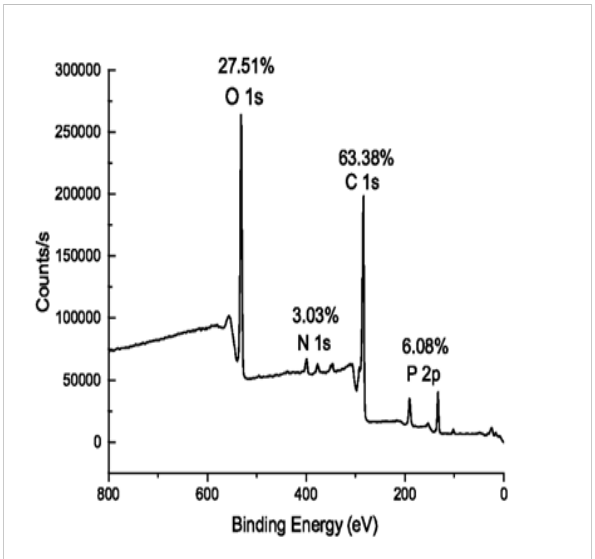

Figure. 3 Survey scan data

understanding of the PC behavior of materials. The surface of PNDC contains varying amounts of carbon, oxygen, nitrogen, and phosphorus, so there are a variety of functional groups that the elements could arrange themselves into. Deconvolution of the N 1s narrow scan spectrum reveals three different nitrogen environments that include pyridinic, (398.8 eV) [33,40–43] pyrrolic, (400.9 eV) [43–46] and N—oxide (404.6) [47,48]. The N—oxide peak is shifted from its usual position andit is generally observed at ~402 eV. Thisis ascribed to the change in the environment when nitrogen is not the only dopant in the carbon matrix. Pyridinic and pyrrolic functionalities are advantageous for many applications such as oxygen reduction reaction (ORR) [43], catalysis [49] and supercapacitors [50]. Doping with nitrogen increases the charge density of neutral carbon atoms that consequently increase the overall reactivity of the PNDC surface [33,51]. Along with nitrogen functionalities, an exceptional amount of phosphorus-containing functional groups were also present on PNDC surface. Two different bonding environments were identified from XPS and determined to be phosphonyl (5.8%) and phosphoric acid (0.3%) groups. Table 3 shows XPS narrow scan data for heteroatom functionalities present on PNDC.

Element, functionality	Peak BE	Atomic %
N1, pyridinic	398.8	0.85
N2, pyrrolic	400.9	1.74
N3, N—oxide	404.6	0.27
O1, quinone	531.1	5.78
O2, carbonyl	532.7	20.8
O3, ether	535.5	2.28
P1, phosphonyl	133.7	5.81
P2, polyphosphoric acid	136.9	0.30

Table 3. Narrow scan data

Raman spectroscopy

In an effort to describe the carbon bonding environment of PNDC, Raman spectroscopy was performed. The characteristic peaks are found at approximately 1600 and 1350 cm^{-1} which correspond to G (graphitic) and D (disorder) bands of sp^2 hybridized carbon respectively. The G band occurs due to stretching motion between sp^2 carbons while the D band is due to a breathing mode that is forbidden between carbons in pristine graphite [24]. The defect ratio, I_D/I_G, provides information on the degree of disorder in a carbon sample which can be very well correlated to the conductivity of the carbon sample. The defect ratio is calculated by peak deconvolution and integration. Spectra were taken at eight different positions and the defect ratio was averaged. An example Raman spectrum for PNDC is shown in Figure. 4. An I_D/I_G value of 1.65 ± 0.1 was obtained, indicating a high degree of doping of PNDC material.

Electrochemical characterization

Electrochemical performance of the material is determined by cyclic voltammetry in acidic and alkaline electrolyte, using a three-electrode cell configuration. In H_2SO_4, voltammograms are quasi-rectangular in shape, similar to other materials that exhibit EDLC characteristics. Figure 5. shows voltammograms of PNDC at varying scan rates from 5 to 90 mV/s.Voltammograms are almost perfectly rectangular in shape at scan rates from 5 to 100 mV/s indicating that classical EDLC and high rate capability [52]. This is due to the high surface area (725 m^2/g) and well-developed pore structure. The surface area of PNDC is high enough to allow adequate electrolyte to contact with the surface of the material. The pores have an average diameter of 3 nm and are mainly mesopores (2-50 nm), with about 32% being micropores. Both mesopores and micropores are highly important in the transporting ability and speed throughout the PNDC.

All voltammograms also exhibit a reversible peak around 0.4 V which is characteristic of faradaic influence. This is due to the PC capability of functional groups on the PNDC surface. XPS results show that the PNDC material contains functionalities on its surface such as pyrrolic, pyridinic, quinone, etc. that can undergo redox reactions with H+ in solution [31]. Some of the possible redox reactions due to heteroatom doping are found in Scheme 1. PNDC is rich with dopants on the surface, with approximately 37% of its surface elemental composition being atoms that are not carbon. The material shows high percentage of doping element at surface, as well as an adequate surface morphology to allow for functional groups to interact with electrolyte ions. These characteristics are attributed to the exceptional capacitance performance on PNDC.

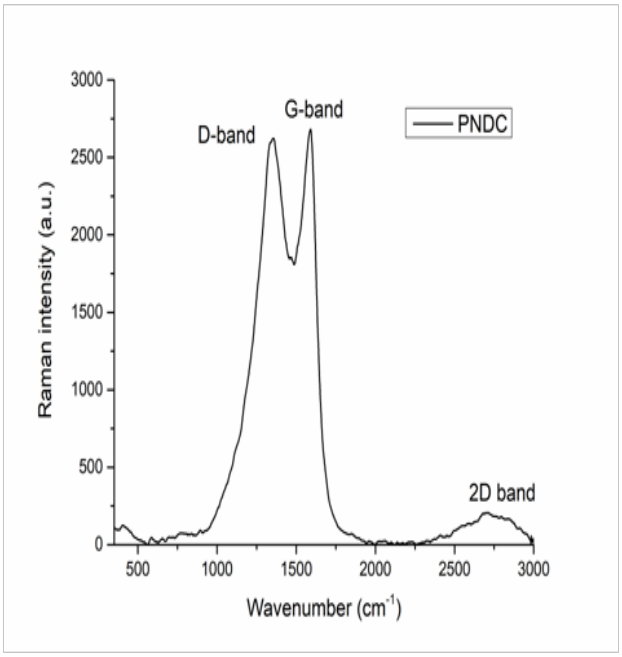

Figure 4. Raman spectra of PNDC

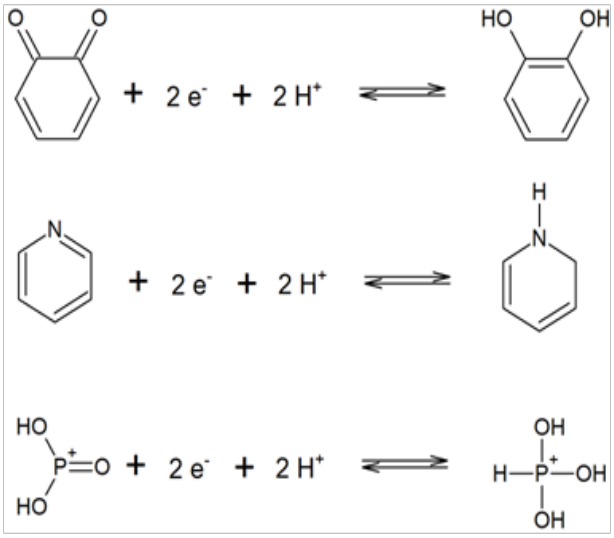

Scheme 1. Possible faradaic redox reactions between surface groups and acidic electrolyte

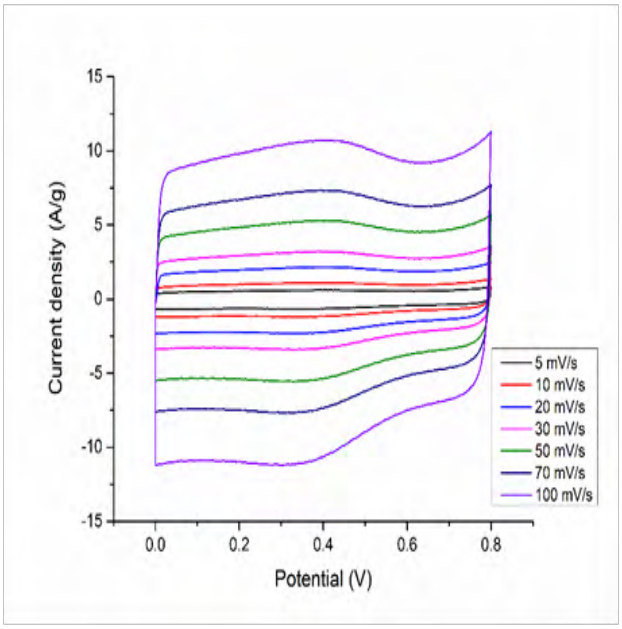

Figure 5. Voltammograms of PNDC in 1 M H_2SO_4 at various scan rates from 5 to 100 mV/s

In alkaline electrolyte, 6M KOH, a Hg/HgO electrode was used as a reference. Voltammograms of PNDC in basic media, like in acid, show an almost perfect rectangular shape. This is illustrated in Figure 6. In contrast, the voltammogram does not contain any redox peak in basic media. However, the specific capacitance value is increased from 156.4 to 182.5 F/g in acid and base electrolyte, respectively. This is likely due to the appropriate size matching of the pores on the surface of PNDC and the hydroxide and potassium ions. It is also worth mentioning that as the scan rate increases, the shape of the voltammogram does not change, which is indicative of electrochemical stability of the PNDC material under alkaline conditions. This shape stability also demonstrates low resistance and efficient ion transport during the charging/discharging process. This can be attributed to the high percentage of mesopores (68%) that operate as transport channels for electrolyte to be diffused into the bulk of the material.

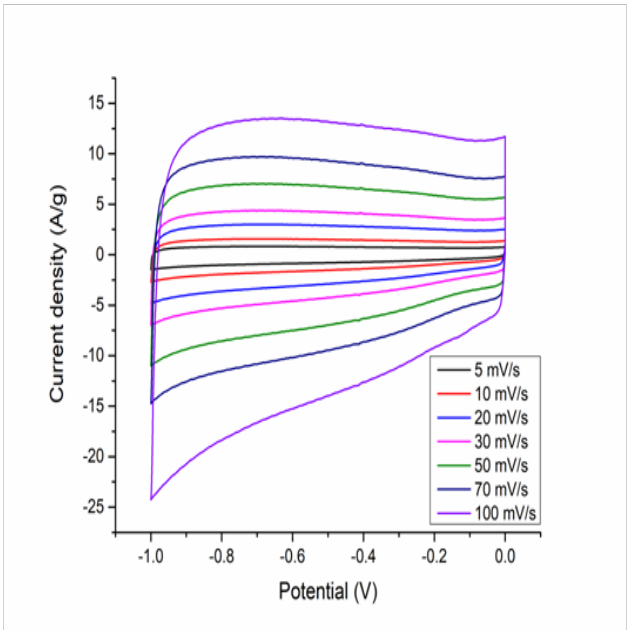

Figure 6.Voltammograms of PNDC in 6 M KOH at various scan rates from 5 to 100 mV/s

The capacitance of the material is directly related to the sweep rate of the potential across the electrode based on the Randles-Sevcik equation. The highest specific capacitance is achieved at 5 mV/s in both electrolytes with values of 156 and 183 F/g for acid and base, respectively. The material retains 83% (acid) and 81% (base) of its specific capacitance from 5 to 100 mV/s, indicating its ability to efficiently store charge even at very rapid scan rates. Figure 7 illustrates this dependence of capacitance on the scan rate.

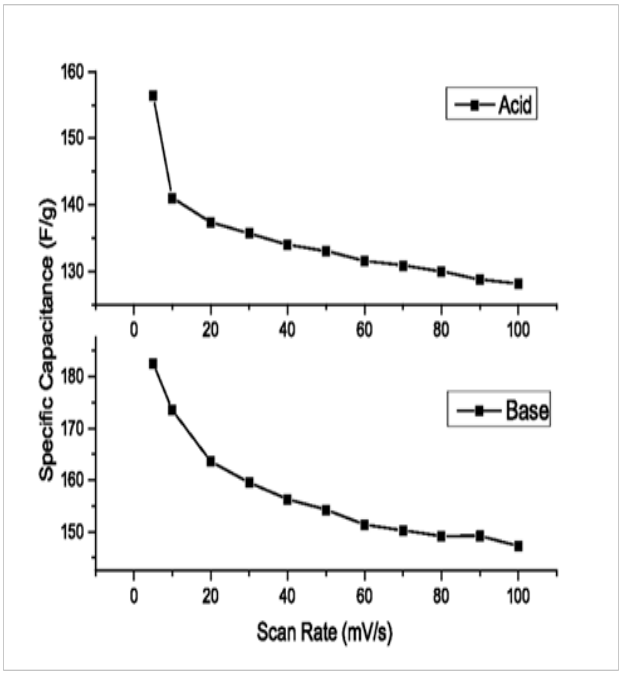

Figure 7.Dependence of capacitance on scan rate

Recyclability

The stability of PNDC as a supercapacitor electrode material was determined by performing 3000 consecutive cycles, of cyclic voltammograms (Figure 8a) Specific capacitance was calculated at various cycle intervals. The results in Figure 8b show that the specific capacitance of the material decreases approximately 5% from zero cycles (155.6 F/g) to 3000 cycles (147.9 F/g). This makes this PNDC material an excellent candidate for a long-lifetime and low-cost electrode material.

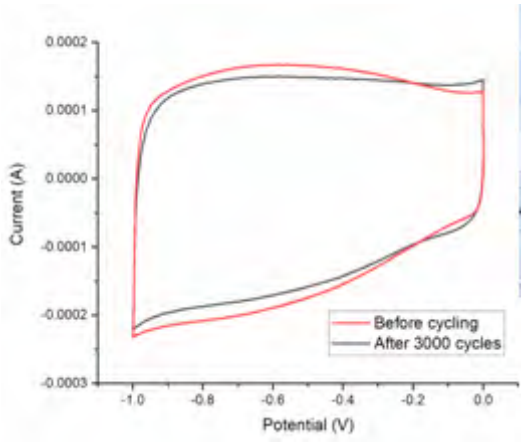

Figure 8. a) Cyclic voltammograms of PNDC at 50 mV/s before and after cycling 3000 times and

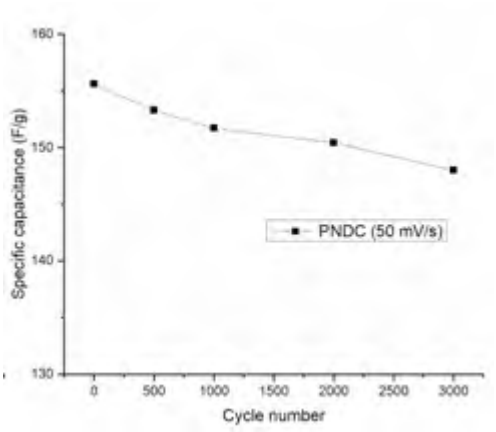

b) Specific capacitance (F/g) of PNDC dependence on cycle number at a scan rate of 50 mV/s

Conclusion

This work illustrates a simple method of generating an economical, renewable, carbon-based electrode coating material. The one-step carbonization can easily be scaled up to industry proportions. PNDC was shown to exhibit exceptional capacitance values of 156 F/g in acidic media and 182 F/g in alkaline media. The electrochemical storage ability of the material is due to its surface characteristics. PNDC has a high surface area of ~724 m^2g^{-1} with a well-developed pore structure and spherical-shaped morphology. The contribution due to PC was linked to the high doping of the surface with nitrogen, phosphorus, and oxygen functionalities such as quinone and pyrrolic groups. PNDC also shows exceptional electrochemical stability, with specific capacitance retention of 95% over 3000 consecutive cycles. Thus, this PNDC material shows to be promising as a renewable and economical electrode material for supercapacitors.

Acknowledgment

The authors would like to acknowledge Shawn Bourdo and the Center for Integrative Nanotechnology Sciences for help with physical characterization of PNDC.

References

1. Burke A, Zhao H (2015) Present and Future Applications of Supercapacitors in Electric and Hybrid Vehicles. in Applications of Supercapacitors in Electric and Hybrid Vehicles 1–5.
2. Hou J, Cao C, Idrees F, Ma X (2015) Hierarchical Porous Nitrogen-Doped Carbon Nanosheets Derived from Silk for Ultrahigh-Capacity Battery Anodes and Supercapacitors.
3. Simon P, Gogotsi Y (2008) Materials for electrochemical capacitors. Nat. Mater 7: 845–854.
4. Lu W, Qu L, Henry K, Dai L (2009) High performance electrochemical capacitors from aligned carbon nanotube electrodes and ionic liquid electrolytes. J. Power Sources 189: 1270–1277.
5. Yun YS, Park HH, Jin HJ (2012) Pseudocapacitive effects of N-doped carbon nanotube electrodes in supercapacitors. Materials (Basel) 5: 1258–1266.
6. Zhai Y, Dou Y, Zhao D, Fulvio PF, Mayes RT, et al. (2011) Carbon materials for chemical capacitive energy storage. Adv. Mater 23: 4828–4850.
7. Oh YJ, Yoo JJ, Kim Y II, Yoon JK, Yoon HN, et al. (2014) Oxygen functional groups and electrochemical capacitive behavior of incompletely reduced graphene oxides as a thin-film electrode of supercapacitor. Electrochim. Acta 116: 118–128.
8. Candelaria SL, Garcia BB, Liu D, Cao G (2012) Nitrogen modification of highly porous carbon for improved supercapacitor performance, J Mater Chem 22: 9884.
9. Hulicova D, Yamashita J, Soneda Y, Hatori H, Kodama M et al. (2005) Supercapacitors Prepared from Melamine-Based Carbon Chem Mater 17: 1241–1247.
10. An KH, Kim WS, Park YS, Choi YC, Lee SM et al. (2001) Supercapacitors Using Single Walled Carbon Nanotube Electrodes. Adv Mater 13: 497–500.
11. Kaempgen M, Chan CK, Ma J, Cui Y, Gruner G et al. (2009) Printable Thin Film Supercapacitors Using Single-Walled Carbon Nanotubes. Nano Lett 9: 1872–1876.
12. Saliger R, Fischer U, Herta C, Fricke J (1998) High surface area carbon aerogels for supercapacitors. J Non Cryst Solids 225: 81–85.
13. Yu M, Li J, Wang L (2017) KOH-activated carbon aerogels derived from sodium carboxymethyl cellulose for high-performance supercapacitors and dye adsorption. Chem Eng J 310: 300–306.
14. Li J, Wang X, Huang Q, Gamboa S, Sebastian PJ (2006) Studies on preparation and performances of carbon aerogel electrodes for the application of supercapacitor. J Power Sources 158: 784–788.
15. Zhang K, Zhang LL, Zhao XS, Wu J (2010) Graphene/polyaniline nanofiber composites as supercapacitor electrodes. Chem Mater 22: 1392–1401.
16. Shao Y, Zhang S, Engelhard MH, Li G, Shao G et al. (2010) Nitrogen-doped graphene and its electrochemical applications. J Mater Chem 20: 7491.
17. Hwang JY, Li M, El-Kady MF, Kaner RB (2017) Next-Generation Activated Carbon Supercapacitors: A Simple Step in Electrode Processing Leads to Remarkable Gains in Energy Density Adv Funct Mater 27.
18. Ramasahayam SK, Clark AL, Hicks Z. Viswanathan T (2015) Spent coffee grounds derived P, N co-doped C as electrocatalyst for supercapacitor applications. Electrochim Acta 168: 414–422.
19. Inal IIG, Holmes SM, Banford A, Aktas Z (2015) The performance of supercapacitor electrodes developed from chemically activated carbon produced from waste tea. Appl Surf Sci 357: 696–703.
20. Marrakchi F, Auta M, Khanday WA, Hameed BH (2017) High-surface-area and nitrogen-rich mesoporous carbon material from fishery waste for effective adsorption of methylene blue. Powder Technol 321: 428–434.
21. Xu G, Tian Z (2017) Walnut shell derived porous carbon for a symmetric all-solid-state supercapacitor. Appl Surf Sci 31: 170–176 .
22. Sun L, Tian C, Fu Y, Yang Y, Yin J et al. (2013) Nitrogen-Doped Porous Graphitic Carbon as an Excellent Electrode Material for Advanced Supercapacitors. Chem A Eur J 20: 564–574.
23. Wang D, Li F, Yin L, Lu X, Chen ZG (2012) Nitrogen-Doped Carbon Monolith for Alkaline Supercapacitors and Understanding Nitrogen-Induced Redox Transitions. Chem A Eur J 18: 5345–5351.
24. Macchi S, Siraj N, Watanabe F, Viswanathan T (2019) Renewable-Resource-Based Waste Materials for Supercapacitor Application. Chemistry Select 4: 492–501.

25. Chen LF, Huang ZH, Liang HW, Gao HL, Yu SH (2014) Three-dimensional heteroatom-doped carbon nanofiber networks derived from bacterial cellulose for supercapacitors. Adv Funct Mater 24: 5104–5111.
26. Mondal AK. Kretschmer K, Zhao Y, Liu H, Fan H et al. (2017) Naturally nitrogen doped porous carbon derived from waste shrimp shells for high-performance lithium ion batteries and supercapacitors. Microporous Mesoporous Mater 246: 72–80.
27. Xiong D, Li X, Fan L, Bai, Z (2018) Three-Dimensional Heteroatom-Doped Nanocarbon for Metal-Free Oxygen Reduction Electrocatalysis: A Review. Catalysts 8: 301.
28. Wang D, Li F, Chen Z, Lu GQ, Cheng, H et al. (2008) Synthesis and Electrochemical Property of Boron-Doped Mesoporous Carbon in Supercapacitor 7195–7200.
29. Zhao BL, Fan LJ, Zhou MQ, Guan H, Qiao S et al (2010)b Nitrogen-Containing Hydrothermal Carbons with Superior Performance in Supercapacitors 5202–5206.
30. Kimn J, Choi M, Ryoo R (2008) Synthesis of Mesoporous Carbons with Controllable N-Content and Their Supercapacitor Properties 29: 13–16.
31. Ramasahayam SK, Hicks Z, Viswanathan T (2015) Thiamine-Based Nitrogen, Phosphorus, and Silicon Tri-doped Carbon for Supercapacitor Applications. ACS Sustain Chem Eng 3: 2194–2202.
32. Ramasahayam SK, Viswanathan T (2016) Honey-Based P, N and Si Tri-Doped Graphitic Carbon Electrocatalysts for Oxygen Reduction Reaction in Alkaline Conditions. Chemistry Select 1: 3527–3534.
33. Gopal Bairi V et al. [2013] Microwave-Assisted Synthesis of Nitrogen and Phosphorus Co-Doped Mesoporous Carbon and Their Potential Application in Alkaline Fuel Cells. Sci Adv Mater 5: 1275–1281.
34. Nasini UB, Bairi VG, Ramasahayam SK, Bourdo SE, Viswanathan T et al. (2014) Oxygen Reduction Reaction Studies of Phosphorus and Nitrogen Co-Doped Mesoporous Carbon Synthesized via Microwave Technique. Chem Electro Chem 1: 573–579.
35. Sing KSW (1985) Reporting physisorption data for gas/solid systems with special reference to the determination of surface area and porosity. Pure Appl Chem 57: 603–619 (1985).
36. Gao S, Chen Y, Fan H, Wei X, Hu C et al. (2014) Large scale production of biomass-derived n-doped porous carbon spheres for oxygen reduction and supercapacitors. J Mater Chem A 2: 3317–3324.
37. Ma X, Liu M, Gan L (2013) Synthesis of micro- and mesoporous carbon spheres for supercapacitor electrode. J Power Sources 17.
38. Kichambare P, Kumar J, Rodrigues S, Kumar B (2011) Electrochemical performance of highly mesoporous nitrogen doped carbon cathode in lithium–oxygen batteries. J Power Sources 196: 3310–3316.
39. Zhang XF, Zhang J, Liu L (2014) Fluorescence Properties of Twenty Fluorescein Derivatives: Lifetime, Quantum Yield, Absorption and Emission Spectra. J Fluoresc 24: 819–826.
40. Wang H, Maiyalagan T, Wang X (2012) Review on Recent Progress in Nitrogen-Doped Graphene: Synthesis, Characterization, and Its Potential Applications. ACS Catal 2: 781–794.
41. Qie L, Chen W, Xu H, Xiong X, Jiang Y et al. (2013) Synthesis of functionalized 3D hierarchical porous carbon for high-performance supercapacitors. Energy Environ Sci 6: 2497.
42. Liu L, Xu SD, Wang FU, Song YJ, Liu J et al. (2017) Nitrogen-doped carbon materials with cubic ordered mesostructure: low-temperature autoclaving synthesis for electrochemical supercapacitor and CO 2 capture. RSC Adv 7: 12524–12533.
43. Jin H, Zhang H, Zhong H, Zhang J (2011) Nitrogen-doped carbon xerogel: A novel carbon-based electrocatalyst for oxygen reduction reaction in proton exchange membrane (PEM) fuel cells. Energy Environ. Sci 4: 3389.
44. Hao YN, Guo HL, Tian L., Kang X (2015) Enhanced photoluminescence of pyrrolic-nitrogen enriched graphene quantum dots. RSC Adv 5: 43750–43755.
45. Hassan FM, Chabot V, Li J, Kim BK, Yu A et al. (2013) Pyrrolic-structure enriched nitrogen doped graphene for highly efficient next generation supercapacitors. J Mater Chem A 1: 2904.
46. Stańczyk K, Dziembaj R, Piwowarska Z, Witkowski S (1995) Transformation of nitrogen structures in carbonization of model compounds determined by XPS. Carbon N. Y 33: 1383–1392.
47. Wicikowski L, Kusz B, Murawski L, Susła B, Szaniawska K (1999) AFM and XPS study of nitrided TiO2 and SiO2–TiO2 sol–gel derived films. Vacuum 54: 221–225.
48. Pietrzak R (2009) XPS study and physico-chemical properties of nitrogen-enriched microporous activated carbon from high volatile bituminous coal. Fuel 88: 1871–1877.
49. Li, X (2019) Pyridinic Nitrogen-Doped Graphene Nanoshells Boost the Catalytic Efficiency of Palladium Nanoparticles for the N -Allylation Reaction. Chem Sus Chem 12: 858–865.
50. Ramasahayam SK, Nasini UB, Shaikh AU, Viswanathan T (2015) Novel tannin-based Si, P co-doped carbon for supercapacitor applications. J Power Sources 275: 835–844.
51. Zhang L, Niu J, Dai L, Xia Z (2012) Effect of Microstructure of Nitrogen-Doped Graphene on Oxygen Reduction Activity in Fuel Cells. Langmuir 28: 7542–7550.
52. Chen LF, Lu Y, Yu L, Lou XW (David) Designed formation of hollow particle-based nitrogen-doped carbon nanofibers for high-performance supercapacitors. Energy Environ Sci 10: 1777–1783.